

# Dispersion of waves in relativistic plasmas with isotropic particle distributions

Roman V. Shcherbakov\*

*Harvard-Smithsonian Center for Astrophysics, 60 Garden Street, Cambridge, MA 02138*

(Dated: January 26, 2009)

The dispersion laws of Langmuir and transverse waves are calculated in the relativistic non-magnetized formalism for several isotropic particle distributions: thermal, power-law, relativistic Lorentzian  $\kappa$ , and hybrid  $\beta$ . For Langmuir waves the parameters of superluminal undamped, subluminal damped principal and higher modes are determined for a range of distribution parameters. The undamped and principal damped modes are found to match smoothly. Principal damped and second damped modes are found not to match smoothly. The presence of maximum wavenumber is discovered above that no longitudinal modes formally exist. The higher damped modes are discovered to be qualitatively different for thermal and certain non-thermal distributions. Consistently with the known results, the Landau damping is calculated to be stronger for non-thermal power-law-like distributions. The dispersion law is obtained for the single undamped transverse mode. The analytic results for the simplest distributions are provided.

## I. INTRODUCTION

The non-thermal distributions of electrons are as important as thermal for astrophysical plasmas. Shocked and turbulent medium is likely to accelerate the electrons into the power-laws. Gamma-Ray bursts<sup>1</sup> (GRBs), jets from compact sources<sup>2</sup>, low luminosity active galactic nuclei<sup>3</sup> (LLAGNs) show evidence of the non-thermal relativistic distributions. The electrons are non-thermal and mildly relativistic near Earth<sup>4</sup> and in solar corona<sup>5</sup>.

The properties of EM waves propagating through such medium are worth knowing even in a non-magnetized case. EM waves can be generated in turbulence, propagate some distance and dump via the Landau damping. Thus energy is redistributed. Whereas the realistic turbulence is non-linear, only the linear waves are considered in this work. No back-reaction of waves on the electron distributions is assumed.

The reasonable relativistic electron distributions are thermal (10), power-law (11), Lorentzian  $\kappa$  (12) and hybrid  $\beta$  (13). They are taken to be normalized to unity when integrated over momenta. I take all the quantities in the paper to be dimensionless for the sake of clarity and brevity. Temperature  $T$  of thermal distribution is evaluated in the units of  $mc^2/k_B$  for the particles with mass  $m$ . Here  $c$  is the speed of light and  $k_B$  is Boltzmann constant. The inverse temperature

$$\rho = \frac{1}{T} \quad (1)$$

is sometimes denoted as  $\mu$  in the literature. Momenta of particles  $p$  is measured in  $mc$ . The speed of light  $c$  is set to unity. Thus

$$\gamma = \sqrt{1 + p^2} \quad (2)$$

is the particles dimensionless energy. The non-relativistic plasma frequency in CGS units (for particles with charge  $q$ )

$$\omega_p = \sqrt{\frac{4\pi n q^2}{m}} \quad (3)$$

is employed to normalize the absolute values of a wavenumber  $k$  and frequency  $\omega$  as<sup>6</sup>

$$\Omega = \frac{\omega}{\omega_p}, \quad \mathbf{K} = \frac{\mathbf{k}}{\omega_p}. \quad (4)$$

The scalar  $K$  is the absolute value of the vector  $\mathbf{K}$ .

The general characteristics of relativistic plasma are the following. Transverse waves have the phase velocity greater than the speed of light  $\Omega/K > 1$  and so are undamped. They only have the single mode. The longitudinal waves exhibit the wider range of phenomena<sup>6,7</sup>. The phase velocity goes from  $> 1$  to  $< 1$  as  $K$  increases, the undamped mode at small  $K$  matches the principal damped mode that exists at higher  $K$  up to  $K_{max}$ .<sup>8</sup> Besides the principal mode, the finite set of higher damped modes exists. The present paper elaborates on all these modes for various isotropic particle distribution. Either a mixture of electrons and positrons with same distributions or immobile ions are considered, so that the ion sound does not appear.

The paper is organized as follows. The formalism of linear plasma dispersion is reviewed in §II. The results of numeric evaluations are presented in §III. Some analytic formulas can be found in §IV. I conclude with the discussion and the summary in §V.

## II. LINEAR DISPERSION LAWS

Waves propagating in plasma feel the plasma response, which can be characterized by the permittivity tensor  $\varepsilon(\mathbf{K}, \Omega)$  in the linear regime. Permittivity tensor<sup>6,9</sup>

$$\varepsilon(\mathbf{K}, \Omega) = 1 + \sum_{species} \frac{1}{\Omega^2} \int \frac{1}{p} \frac{\partial f}{\partial p} \frac{\mathbf{p}\mathbf{p}}{\gamma - \mathbf{K} \cdot \mathbf{p}/\Omega} d^3p \quad (5)$$

leads<sup>6,10</sup> after the integration over the polar angles to longitudinal permittivity

$$\varepsilon_L = \frac{2\pi^2 i \sigma \Omega}{K^3} \int_{\gamma_0}^{\infty} \frac{\partial f}{\partial \gamma} \gamma^2 d\gamma + 1 \quad (6)$$

$$- \frac{2\pi}{\Omega K} \int_0^{\infty} p^2 \frac{\partial f}{\partial p} \left\{ \frac{2\gamma\Omega}{Kp} + \frac{\gamma^2\Omega^2}{K^2 p^2} \ln \left[ \frac{\gamma\Omega - Kp}{\gamma\Omega + Kp} \right] \right\} dp$$

and transverse permittivity

$$\varepsilon_T = 1 + \frac{\pi^2 i \sigma}{\Omega K} \int_{\gamma_0}^{\infty} \frac{\partial f}{\partial \gamma} \left( 1 - \frac{\gamma^2}{\gamma_0^2} \right) d\gamma + \quad (7)$$

$$\frac{\pi}{\Omega K} \int_0^{\infty} p^2 \frac{\partial f}{\partial p} \left\{ \frac{2\gamma\Omega}{Kp} + \left( \frac{\gamma^2\Omega^2}{K^2 p^2} - 1 \right) \ln \left[ \frac{\gamma\Omega - Kp}{\gamma\Omega + Kp} \right] \right\} dp,$$

where  $\gamma_0 = (1 - \Omega^2/K^2)^{-1/2}$ . The Landau rule is applied, so that  $\sigma = 0$  for  $\text{Re}[\Omega^2] \geq K^2$  and for  $\text{Re}[\Omega^2] < K^2$  one has<sup>6</sup>

$$\sigma = \begin{cases} 0 & \text{for } \text{Im}[\Omega] > 0, \\ 2 & \text{for } \text{Im}[\Omega] < 0. \end{cases} \quad (8)$$

The case with  $\text{Im}[\Omega] = 0$  for  $\text{Re}[\Omega^2] < K^2$  is unphysical<sup>11</sup>. Only one sort of species is considered in the above formulas without the loss of generality. The plasma density  $n$  is that of the mobile species in the case of immobile ions or the total density for electron-positron plasma.

### III. NUMERIC RESULTS

The dispersion laws  $\Omega(K)$  of waves propagating in plasma are determined as solutions of the equations

$$\varepsilon_L = 0, \quad \varepsilon_T = \frac{K^2}{\Omega^2}. \quad (9)$$

#### A. Thermal distribution

The thermal relativistic distribution of particles

$$f_T(p) = \frac{\rho \exp(-\rho\gamma)}{4\pi K_2(\rho)} \quad (10)$$

describes highly collisional relaxed plasma. Here and below  $K_n$  represents  $n$ -th modified Bessel function of the second kind.

The longitudinal waves in thermal plasma have variety of features. The non-relativistic theory<sup>12</sup> predicts the infinite number of damped modes, whereas the relativistic analysis<sup>7</sup> limits the damped modes to a finite set. In addition, the superluminal undamped part of the spectrum appears. The boundary  $K$  for these modes are shown on Fig. 1. These are the solutions of the dispersion relation (9) for real  $\Omega$  and  $K$ . The transition between the damped (high  $K$ ) and undamped (low  $K$ ) modes is indicated by

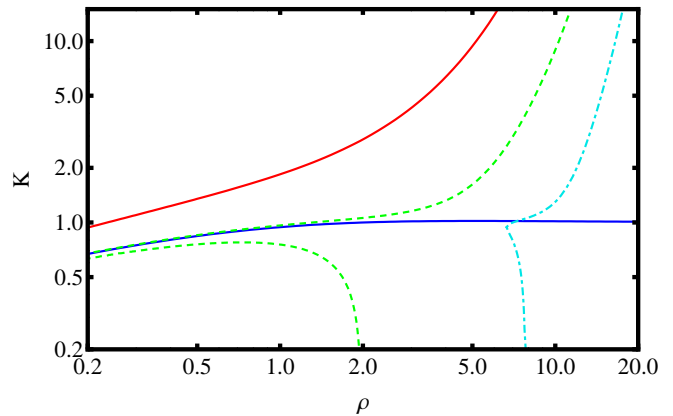


FIG. 1: (Color online) Upper solid (red) - maximum  $K$  for principal damped longitudinal harmonic, lower solid (blue) - for undamped harmonic; dashed (green) -  $K$  boundaries for second damped harmonic, dot-dashed (cyan) - for third damped harmonic.

the lower solid blue line. The principal damped mode exists for  $K$  limited by the upper solid red line, whose  $K$  grows exponentially fast as  $T \rightarrow 0$ . No modes formally exist above that line, as the ion sound is absent. However, the calculations in this large- $K$  area are unphysical, because the set of particles constituting plasma does not behave coherently at very low wavenumbers, as the wavelength approaches the particle effective mean free path about Debye radius  $\lambda_D$ . Thus the branch ceases to exist at wavenumbers  $k \gtrsim 1/\lambda_D$ <sup>13</sup>. Every realization of the distribution function  $f(p)$  gives rise to different evolution of the imposed initial condition. The dashed green lines indicate the upper and lower limiting  $K$  for the second damped mode. This mode exists for any temperature. Its region of allowed  $K$  overlaps with that for the principal mode. The lower limiting  $K$  goes to 0 at  $\rho \sim 2$  and is zero for higher  $\rho$  (lower temperature). The same is true for the third damping mode (boundaries in dot-dashed cyan): the lower limiting  $K$  goes to 0 at  $\rho \sim 8$ . The third damped mode exists only for  $\rho > 6.7$ .

The mode completion effect was claimed to exist by Schlikeiser<sup>7</sup>. It consists of the smooth transition of  $\text{Re}(\Omega(K))$  between the principal and second damped modes. This is quite surprising given the fact that  $\text{Im}(\Omega(K))$  is discontinuous, thus  $\Omega(K)$  is discontinuous. The careful analysis shows that the real part is also discontinuous. The real and imaginary parts of  $\Omega(K)$  for  $\rho = 2$  are shown on Fig. 2 (see Fig. 3 in Ref. (7) for comparison). In agreement with  $K$ -overlapping of the principal and second damped modes (Fig. 1),  $K_{\text{max}} \approx 1.060$  for the second damped modes is larger than  $K_{\text{min}} \approx 1.000$  for the principal damped mode. Thus, the mode completion effect does not occur.

The isocontours of constant  $\text{Re}(\Omega)$  and  $-\text{Im}(\Omega)$  for the principal mode are shown on, respectively, Fig. 3 and Fig. 4. These are the extensions of Figs. 6 and

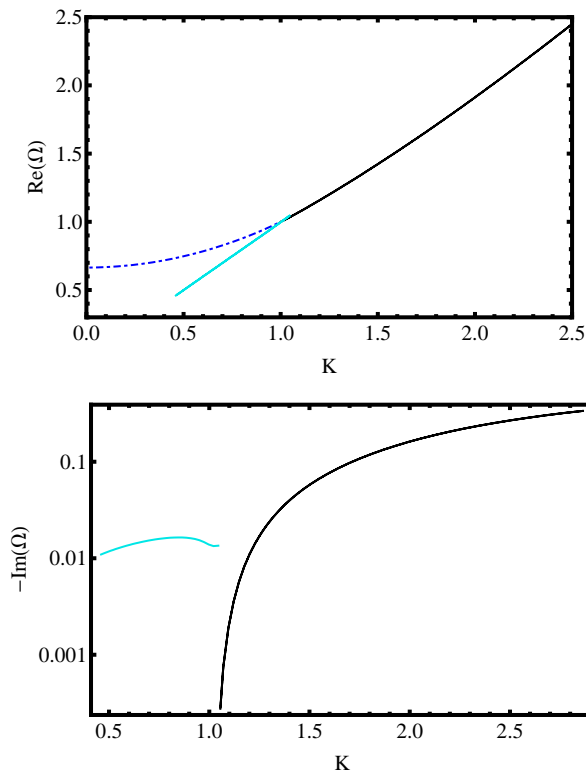


FIG. 2: (Color online) Dispersion relation for longitudinal waves for  $\rho = 2$ . Undamped mode is dot-dashed (blue), principal damped mode is dark solid (black), second damped mode is light solid (cyan).

7 in Ref. (6) to higher temperatures (lower  $\rho$ ) with the maximum  $K$  boundary (see Fig. 1) employed. No modes formally exist below the dark solid line denoted by "max(K)". The modes are undamped to the left from the light solid cyan line " $\Omega = K, \text{Im}(\Omega) = 0$ " and damped to the right. The plasma frequency at the infinite wavelength is shown in dashed green. The correspondent plot for the transverse waves is given in Ref. (6) along with the approximations.

### B. Power-law distribution

The distribution

$$f_P(p) = \frac{\Gamma(\kappa)}{\pi^{3/2}\Gamma(\kappa - \frac{3}{2})} \gamma^{-2\kappa} \quad (11)$$

represents a simplest  $f(p)$ . Also, it produces many analytic results (see §IV). It is often used to interpret the results of astronomical observations of jets<sup>2</sup> or any object where shock acceleration takes place. In applications this distribution is usually applied with the limited range of  $\gamma$ , but for my calculation the entire range of  $\gamma$  is taken.

The migration of critical points of longitudinal dispersion relation is shown on Fig. 5. The superluminal mode

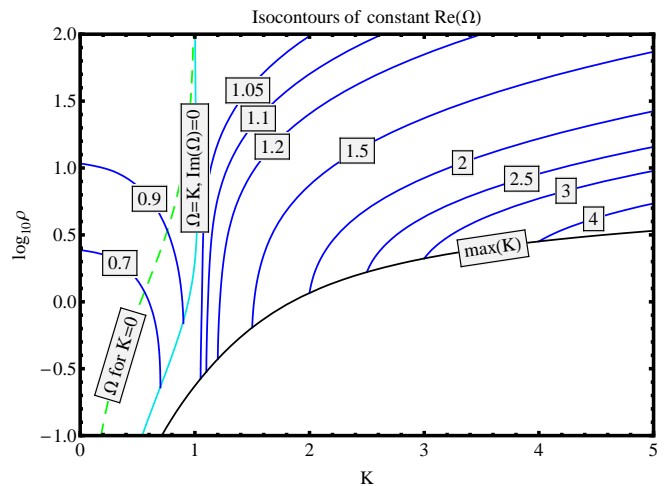


FIG. 3: (Color online) Dispersion contours for longitudinal waves, showing  $\text{Re}(\Omega)$  in  $(K, \log_{10} \rho)$  plane (solid blue lines), zero damping boundary (light solid cyan line), maximum  $K$  curve (dark solid black line),  $\Omega$  as a function of  $\rho$  for  $K = 0$  (dashed green line).

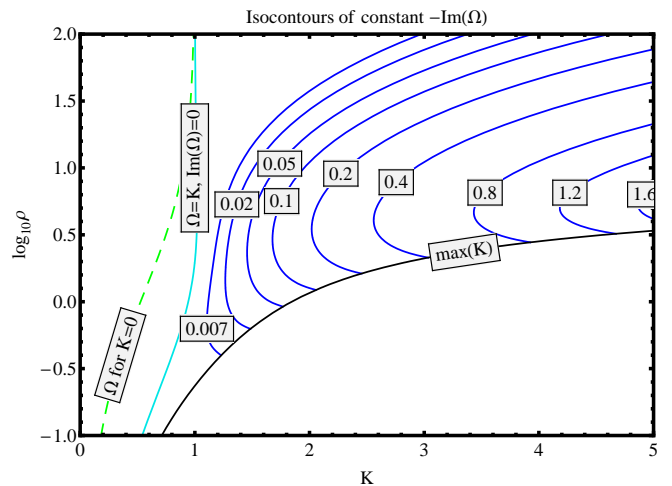


FIG. 4: (Color online) Dispersion contours for longitudinal waves, showing  $-\text{Im}(\Omega)$  in  $(K, \log_{10} \rho)$  plane (solid blue lines), zero damping boundary (light solid cyan line), maximum  $K$  curve (dark solid black line),  $\Omega$  as a function of  $\rho$  for  $K = 0$  (dashed green line).

smoothly converts to a damped principal mode at critical  $K$  about 1, shown in solid blue on the figure. The maximum  $K$  of the principal mode (dashed black curve) grows exponentially fast as a function of  $\kappa$  similarly to the behavior of maximum  $K$  boundary for the thermal distribution Fig. 1. The behavior of higher damped modes is, in contrast, different. The second damped mode appears at  $\kappa = 4.58$ . At higher  $\kappa$  second damped mode can assume  $K$  from 0 to a critical  $K$ , shown in dot-dashed green on the figure. The presence of the second and higher order damped modes at  $K = 0$  is a feature of the power-law distribution and is not observed for the thermal distribu-

tion.

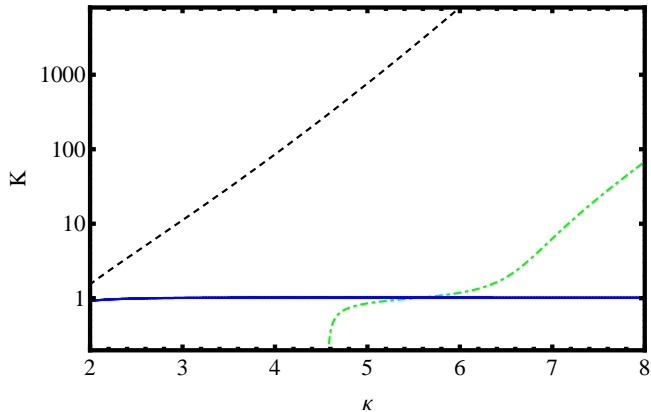


FIG. 5: (Color online) Maximum  $K$  for principal damped longitudinal mode (dashed black line), for second damped mode (dot-dashed green line), for undamped mode (solid blue line).

The isocontours of constant  $\text{Re}(\Omega)$  and  $-\text{Im}(\Omega)$  for the principal mode are shown on, respectively, Fig. 6 and Fig. 7. The chosen small range of  $\kappa \in [2, 3]$  reflects the astronomical need to consider distributions  $N(\gamma) \sim \gamma^{-x} d\gamma$  for  $\gamma \gg 1$  with  $x \in [2, 4]$ . As in the case of thermal plasma, no modes formally exist below the solid black line denoted by "max(K)". The modes are undamped to the left from the light solid cyan line " $\Omega = K, \text{Im}(\Omega) = 0$ " and damped to the right. The plasma frequency at the infinite wavelength is shown in dashed green. The isocontour  $K$  appears to depend only weakly on  $\kappa$ , however the isocontour  $-\text{Im}(\Omega)$  values (Fig. 7) are at least 1.5 times larger for the same  $K$ , than in case of thermal distribution (Fig. 4). The comparison of damping coefficients for thermal and hybrid distributions is given in the next subsection.

### C. Hybrid distribution

I choose the relativistic isotropic Lorentzian  $\kappa$  distribution<sup>4,14</sup>

$$f_H(p) \propto \left( 1 + \frac{\sqrt{1+p^2} - 1}{\kappa\theta^2} \right)^{-(\kappa+1)}, \quad (12)$$

which tends to relativistic thermal distribution with  $T = \theta^2$  as  $\kappa$  approaches infinity. The normalization coefficient is calculated numerically from the condition  $\int_0^\infty 4\pi p^2 f_H(p) dp = 1$ . This distribution is the realistic choice when the acceleration of particles is balanced by the relaxation processes: almost thermal distribution at high  $\kappa$  and almost power-law at low  $\kappa$ . Thus, it is possible to compare the wave propagation for thermal, slightly non-thermal and highly non-thermal distributions.

The comparison of distributions is made on Fig 8. The inverse temperature  $\rho$  for  $f_T(p)$  and the temperature-like parameter  $\theta^2$  for  $f_H(p)$  are chosen in such a way

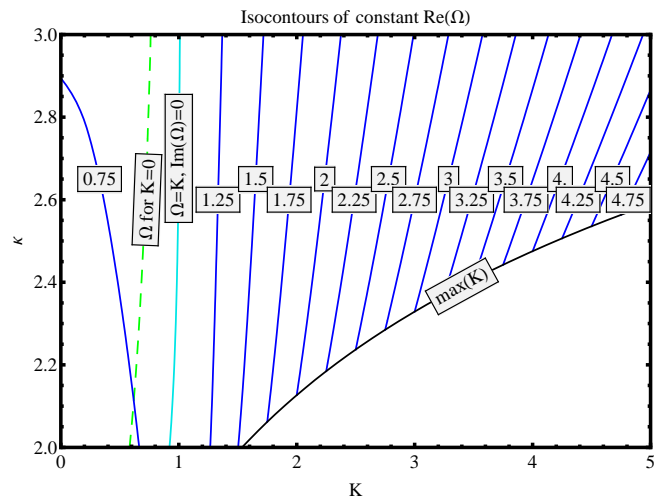


FIG. 6: (Color online) Dispersion contours for longitudinal waves, showing  $\text{Re}(\Omega)$  in the  $(K, \kappa)$  plane (solid blue lines), zero damping boundary (light solid cyan line), maximum  $K$  curve (dark solid black line),  $\Omega$  as a function  $\kappa$  for  $K = 0$  (dashed green line).

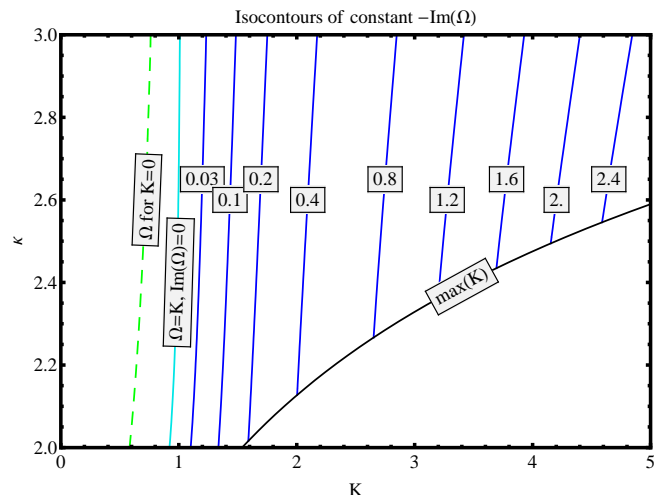


FIG. 7: (Color online) Dispersion contours for longitudinal waves, showing  $-\text{Im}(\Omega)$  in the  $(K, \kappa)$  plane (solid blue lines), zero damping boundary (light solid cyan line), maximum  $K$  curve (dark solid black line),  $\Omega$  as a function  $\kappa$  for  $K = 0$  (dashed green line).

that the average kinetic energy of particle  $E_K = \int (\gamma - 1) 4\pi p^2 f(p) dp$  is equal to 1. The choice of constant  $E_K = 1$  is made to show the typical behavior of dispersion relations for plasmas with approximately the same energetics. The thermal distribution is shown in dot-dashed black. The transition from light green to dark blue corresponds to the increase of  $\kappa$  through the discrete set  $\kappa = 4.5, 5, 5.5, 6, 7, 10, 20$ . The relativistic Lorentzian  $\kappa$  distribution appears to have more particles at lower  $\gamma \approx 1.2$  and higher  $\gamma \gtrsim 5$ , but fewer particles in the intermediate region  $\gamma \sim 3$ . For the contrast I added the

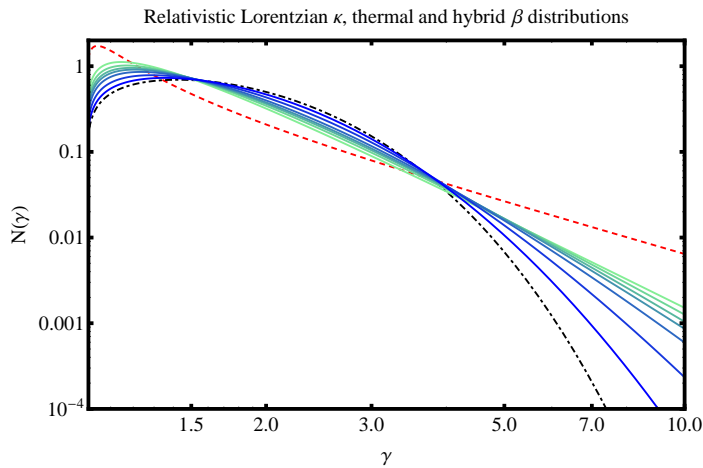


FIG. 8: (Color online) Distributions of particles with kinetic energy  $E_K = 1$ : thermal ( $\kappa \rightarrow \infty$ ) (dot-dashed black line), Lorentzian  $\kappa$  with  $\kappa = 4.5, 5, 5.5, 6, 7, 10, 20$  (light green to dark blue lines), hybrid  $\beta$  distribution (infinite  $E_K$ ) (dashed red line).

hybrid  $\beta$  distribution

$$f_{H2}(p) = \frac{\beta^3}{\pi^2(1 + \beta^2 p^2)^2} \quad (13)$$

with  $\beta = 2$  that is shown by the dashed red line. It was not normalized to  $E_K = 1$ , since it has the divergent total energy. However, the dispersion laws exist for it.

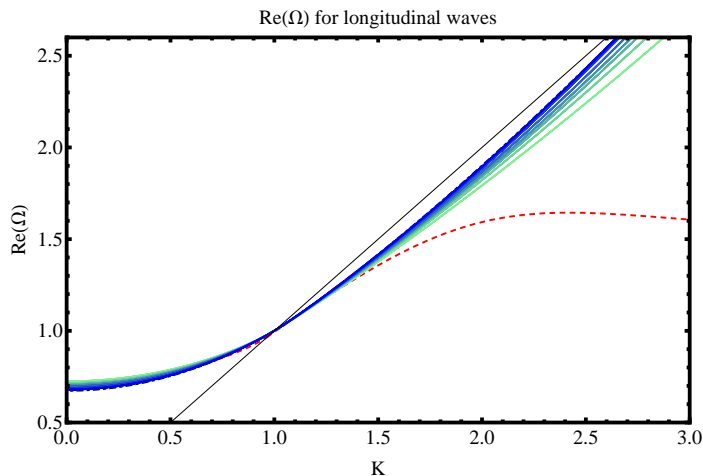


FIG. 9: (Color online)  $\text{Re}(\Omega(K))$  dependence for longitudinal waves for Lorentzian  $\kappa$  distribution: limiting thermal case ( $\kappa \rightarrow \infty$ ) (dot-dashed black line), various  $\kappa$  from 4.5 to 20 (light green to dark blue lines), hybrid  $\beta$  distribution (dashed red line).

The dependencies of  $\text{Re}(\Omega(K))$  for longitudinal waves,  $-\text{Im}(\Omega(K))$  for longitudinal waves and  $\Omega(K)$  for transverse waves are shown for principal modes on, respectively, Fig. 9, Fig. 10, Fig. 11. The thin black line on Fig. 9 separates the undamped mode (on the left) from

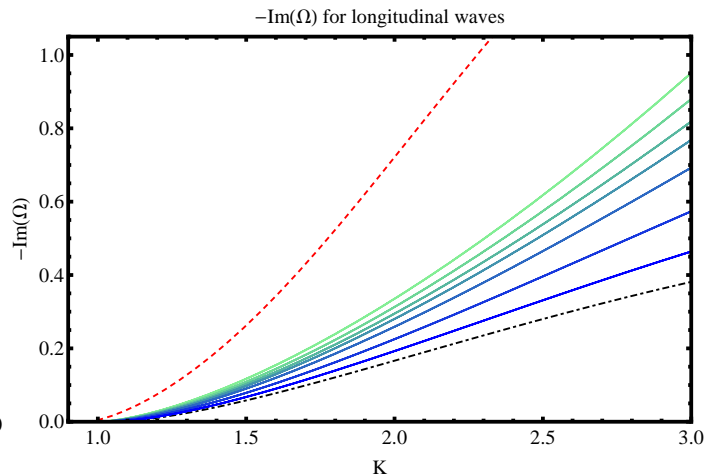


FIG. 10: (Color online)  $-\text{Im}(\Omega(K))$  dependence for longitudinal waves for Lorentzian  $\kappa$  distribution: limiting thermal case ( $\kappa \rightarrow \infty$ ) (dot-dashed black line), various  $\kappa$  from 4.5 to 20 (light green to dark blue lines), hybrid  $\beta$  distribution (dashed red line).

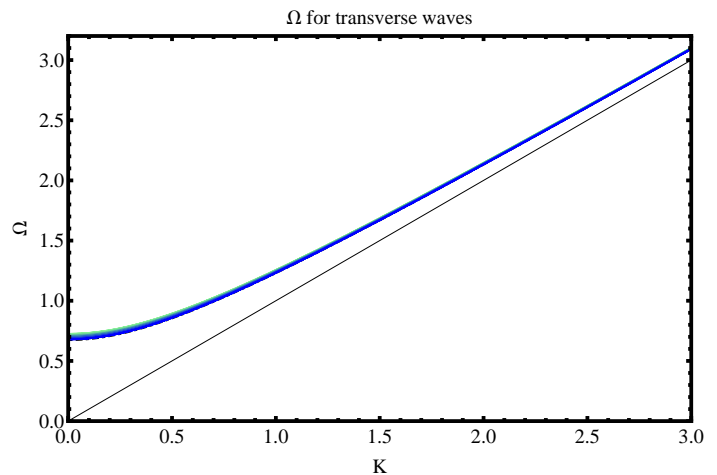


FIG. 11: (Color online)  $\text{Re}(\Omega(K))$  dependence for transverse waves for Lorentzian  $\kappa$  distribution: limiting thermal case ( $\kappa \rightarrow \infty$ ) (dot-dashed black line), various  $\kappa$  from 4.5 to 20 (light green to dark blue lines), hybrid  $\beta$  distribution (dashed red line).

the damped one (on the right). The long-wavelength behavior of longitudinal modes is predictable: more mobile lower  $\gamma$  species in thermal distribution have the lowest plasma frequency. By the same reason  $\Omega$  at  $K = 0$  for transverse waves (Fig. 11) is larger for smaller  $\kappa$ . The variation of  $\text{Re}(\Omega)$  is within 20% for both longitudinal and transverse waves. The Landau damping (Fig. 10) shows larger variation of up to 3 times. The electrons responsible for Landau damping mainly have high  $\gamma \gtrsim 5$ , what makes distributions with smaller  $\kappa$  dissipate waves more effectively. The similar result is observed for non-relativistic Lorentzian  $\kappa$  distribution<sup>15</sup>. The behavior of plasma waves for hybrid  $\beta$  distribution is very different

from that for thermal or Lorentzian  $\kappa$  distribution.

#### IV. ANALYTIC FORMULAS

##### A. Thermal distribution

The Trubnikov's form<sup>16</sup> of the dielectric tensor reads

$$\varepsilon_{\mu\nu} = \delta_{\mu\nu} + \frac{i}{\Omega^2} \frac{\rho^2}{K_2(\rho)} \int_0^\infty d\alpha \left( \frac{K_2(r)}{r^2} \delta_{\mu\nu} - \alpha^2 \frac{K_\mu K_\nu}{\Omega^2} \frac{K_3(r)}{r^3} \right), \quad (14)$$

where

$$r = \left[ \rho^2 - 2i\alpha\rho + \alpha^2 \left( \frac{K^2}{\Omega^2} - 1 \right) \right]^{1/2}. \quad (15)$$

I denote

$$\Delta = 1 - \frac{K^2}{\Omega^2} \quad (16)$$

and expand the Bessel functions in equation (14) in series in  $\Delta$ . The resultant integrals can be evaluated analytically knowing that

$$\int_0^\infty d\alpha \left[ \alpha^n \frac{K_m(\sqrt{\rho^2 - 2i\rho\alpha})}{(\rho^2 - 2i\rho\alpha)^{m/2}} \right] = n! i^{n+1} \frac{K_{n-m+1}(\rho)}{\rho^m}. \quad (17)$$

Then the implicit formula for  $\Delta$

$$\Delta = \Omega^{-2} \sum_{j=0}^{\infty} \left( -\frac{\Delta}{2\rho} \right)^j \frac{(2j)!}{j!} \frac{K_{j-1}(\rho)}{K_2(\rho)} \quad (18)$$

can be derived<sup>9</sup>. It can be rewritten as the explicit formula for  $\Delta$ . The expression for the transverse permittivity

$$\varepsilon_T = 1 - \Delta = 1 - \sum_{n=0}^{\infty} \Omega^{-2(n+1)} \prod_{l=0}^n \frac{K_{l-1}(\rho)}{K_2(\rho)} \frac{(2l)!}{(-2\rho)^l l!} \quad (19)$$

can easily give the dependence  $K(\Omega)$ . Taking  $n = 0$  one obtains

$$\Omega^2 = K^2 + \frac{K_1(T^{-1})}{K_2(T^{-1})} \quad (20)$$

in a high-frequency limit  $\Omega \gg 1$ , coincident with the expression in Ref. (10). As the frequency goes down, terms with higher  $n$  become important. The consecutive approximations are expected to work well for any temperature. The author believes this elegant derivation of the high-frequency approximation was not previously outlined.

##### B. Power-law distribution

The permittivity tensor for the power-law distribution (11) of particles can be calculated analytically.

##### 1. General case

The permittivity components are

$$\begin{aligned} \varepsilon_L = 1 + \frac{2\Gamma(\kappa - 1)}{\Gamma(\kappa + \frac{1}{2})\Gamma(\kappa - \frac{3}{2})K^2} & \left\{ \Gamma(\kappa + 1) \right. \\ & - \kappa \csc(\pi\kappa) \left[ \sqrt{\pi}(1 - \Delta)^{\frac{1}{2} - \kappa} \Delta^{\kappa - 1} \Gamma\left(\kappa + \frac{1}{2}\right) \right. \\ & + \pi \left(\kappa - \frac{1}{2}\right) \left( {}_2\tilde{F}_1\left(2, -\frac{1}{2}, 2 - \kappa, \Delta\right) \right. \\ & \left. \left. - {}_3\tilde{F}_1\left(1, -\frac{1}{2}, 2 - \kappa, \Delta\right) \right) \right] \\ & \left. + \sqrt{\pi} \Delta^{\kappa - 1} (\Delta - 1)^{\frac{1}{2} - \kappa} \kappa \sigma \Gamma\left(\kappa + \frac{1}{2}\right) \right\}, \end{aligned} \quad (21a)$$

$$\begin{aligned} \varepsilon_T = 1 - \frac{\Gamma(\kappa - 1)}{2\Gamma(\kappa + \frac{1}{2})\Gamma(\kappa - \frac{3}{2})K^2} & \left\{ 2\Gamma(\kappa + 1) \right. \\ & - \csc(\pi\kappa) \left[ 2\sqrt{\pi} \Delta^{\kappa} (1 - \Delta)^{\frac{1}{2} - \kappa} \Gamma\left(\kappa + \frac{1}{2}\right) \right. \\ & + \pi\kappa(2 - 3\Delta - 2\kappa) {}_2\tilde{F}_1\left(1, -\frac{1}{2}, 2 - \kappa, \Delta\right) \\ & + 2\pi(\Delta\kappa + \kappa - 1) {}_2\tilde{F}_1\left(2, -\frac{1}{2}, 2 - \kappa, \Delta\right) \left. \right] \\ & \left. - 2\sqrt{\pi} \Delta^{\kappa} (\Delta - 1)^{\frac{1}{2} - \kappa} \sigma \Gamma\left(\kappa + \frac{1}{2}\right) \right\}, \end{aligned} \quad (21b)$$

where  $\sigma$  is determined by Landau rule (see equation (8) and discussion therein). The notation  ${}_2\tilde{F}_1$  represents the regularized hypergeometric function. For the integer  $\kappa$  the limit of  $\kappa$  going to that singular integer value should be considered. The non-singular expressions were also derived, but are longer and are not provided here. The Mathematica 6 convention of branch cuts should be used to evaluate the values of roots and non-integer powers. It sets the branch cuts to be on  $\arg(z) = \pi$  line in the complex  $z$  plane.

The high-frequency limit for the transverse waves is

$$\Omega^2 = K^2 - \frac{\pi \csc(\pi\kappa) \Gamma(\kappa)}{\Gamma(2 - \kappa) \Gamma(\kappa - \frac{3}{2}) \Gamma(\kappa + \frac{1}{2})}. \quad (22)$$

Again the limit must be considered for integer  $\kappa$ .

##### 2. Special cases

Much shorter formulas for permittivities can be derived for certain  $\kappa$ . The shortest ones are for  $\kappa$  in the observationally motivated range  $\kappa \in [2, 3]$ . Let me choose  $\kappa = 2$  and  $\kappa = 5/2$  as the examples.

The case  $\kappa = 2$  (equivalent to  $dN(\gamma) \sim \gamma^{-2} d\gamma$  at high

$\gamma$ ) leads to

$$\varepsilon_T = 1 + \frac{(4 - 10\Delta)\sqrt{\Delta - 1} + 3\sigma\pi\Delta^2 + 6\Delta^2\text{arcsec}(\sqrt{\Delta})}{3\pi K^2(\Delta - 1)^{3/2}}, \quad (23a)$$

$$\varepsilon_L = 1 + \frac{(8 + 16\Delta)\sqrt{\Delta - 1} + 12\sigma\pi\Delta^2 - 24\Delta\text{arcsec}(\sqrt{\Delta})}{3\pi K^2(\Delta - 1)^{3/2}}. \quad (23b)$$

The case  $\kappa = \frac{5}{2}$  (equivalent to  $dN(\gamma) \sim \gamma^{-3}d\gamma$  at high  $\gamma$ ) leads to

$$\varepsilon_T = 1 + \pi \frac{\Delta(10 - 15\Delta + 8\Delta^{3/2}(1 - 2\sigma)) - 3}{16K^2(\Delta - 1)^2}, \quad (24a)$$

$$\varepsilon_L = 1 + 5\pi \frac{\Delta(6 + 3\Delta - 8\Delta^{1/2}(1 - 2\sigma)) - 1}{16K^2(\Delta - 1)^2}. \quad (24b)$$

The longitudinal dispersion relation (24b) for  $\kappa = 5/2$  remarkably gives the compact analytic form for  $\Omega(K)$ . The undamped mode at low  $K$  exists in this case along with the single damped mode at higher  $K$  as

$$\Omega = \frac{1}{8} \sqrt{48K^2 + 5\pi + \sqrt{\frac{(5\pi - 16K^2)^3}{5\pi}}} \quad (25a)$$

for  $K = 0 \dots \frac{\sqrt{5\pi}}{4}$ ,

$$\Omega = \frac{1}{8} \sqrt{48K^2 + 5\pi - i \sqrt{\frac{(16K^2 - 5\pi)^3}{5\pi}}} \quad (25b)$$

for  $K = \frac{\sqrt{5\pi}}{4} \dots \frac{1}{4} \sqrt{5\pi(9 + 4\sqrt{5})}$ .

The relation  $\Omega(K)$  can be expanded near the point  $K_x = \sqrt{5\pi}/4$  to give the powers of  $(K_x - K)^{3/2}$  so that  $\Omega_K$  stays real for  $K < K_x$  and gains the imaginary part for  $K > K_x$ . The second derivative of  $\Omega(K)$  is discontinuous at  $K_x$ . The explicit dispersion law  $\Omega(K)$  (25) is plotted for  $\kappa = 5/2$  on Fig. 12.

### C. Hybrid $\beta$ distribution

The analytic expressions for transverse and longitudinal permittivities need some terms to be abbreviated for brevity in the case of hybrid  $\beta$  distribution (13). They read

$$\varepsilon_T = 1 + \frac{\beta}{\pi A^3 B C K^2} \left[ C(2AB + \beta^4((B - 2C^2) \times \arctan A - B \text{arcsec} \beta)) - 2A^3 \Delta^2 \text{arctanh} C \right] - \frac{\Delta^2 \beta \sigma i}{B C K^2}, \quad (26a)$$

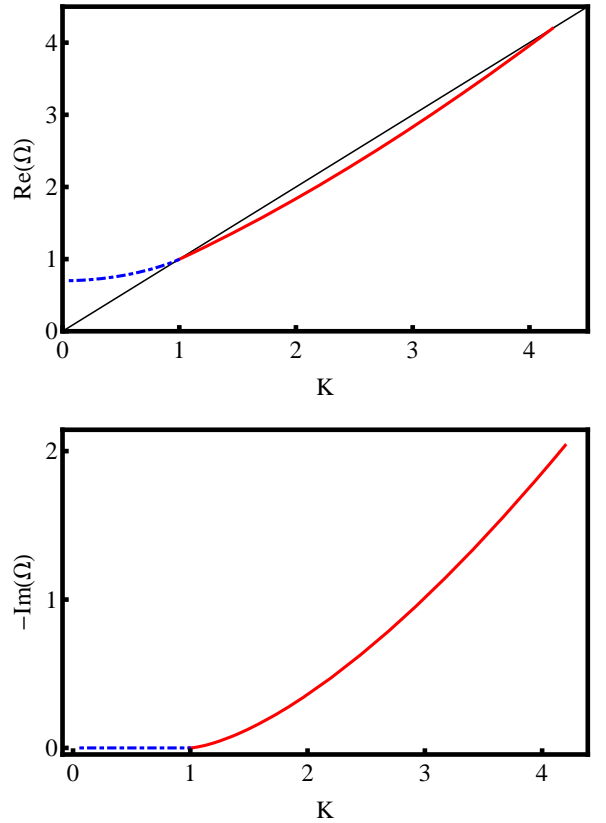


FIG. 12: (Color online) Longitudinal dispersion law for  $\kappa = 5/2$ : undamped mode (dot-dashed blue line), damped mode (solid red line), separated by  $\text{Re}(\Omega) = K$  (thin black line).

$$\varepsilon_L = 1 + \frac{2\beta}{\pi A^3 B^2 C K^2} \left[ B^2 C \beta^4 \text{arcsec} \beta - AC \times (B(B + \Delta A^2) + A\beta^4(B + 2C^2) \arctan A) + 2A^3 \Delta(B + C^2 \beta^2) \text{arctanh} C \right] - \frac{2\beta \Delta \sigma i (B + C^2 \beta^2)}{B^2 C K^2}, \quad (26b)$$

where

$$A = \sqrt{\beta^2 - 1}, \quad B = \beta^2 - \Delta, \quad C = \sqrt{1 - \Delta}. \quad (26c)$$

The expressions for  $\beta = 1$  coincide with those for the power-law distribution with  $\kappa = 2$ .

## V. DISCUSSION & CONCLUSION

The paper derives and reconsiders the broad range of linear wave effects in non-magnetized one species plasma. The various distributions are employed for comparison and to consider the realistic non-equilibrium plasmas. The thermal (10), power-law (11), relativistic Lorentzian  $\kappa$  (12) and hybrid  $\beta$  (13) distributions are employed with the possible inclusion of the simulated distributions<sup>17</sup> in the future.

For longitudinal waves the maximum  $K$  was found to exist above that neither the undamped mode nor the damped mode survive. The mode completion effect<sup>7</sup> was closed. The regions of the principal and the second damped modes overlap in the temperature-wavenumber plane for thermal plasma. The second damped mode always exist. The lower possible  $K$  is zero for low temperatures for second and third damped modes, but is non-zero for higher temperatures. In contrast, for the power-law distribution (11) the second damped mode does not exist for low  $\kappa$ . When it exists at higher  $\kappa$ , its lowest  $K$  is always zero.

Some analytic results are derived that can accelerate the calculations and provide some insight. The full analytic result for longitudinal  $\Omega(K)$  was derived for the power-law distribution (11) with  $\kappa = 5/2$ . The transition

at  $K_x$  between the undamped mode and the principle damped mode was found to be smooth with discontinuous second derivative of  $\Omega(K)$  because of  $(K_x - K)^{3/2}$  term.

### Acknowledgments

The author is grateful to Ramesh Narayan for fruitful discussions and to anonymous referee, whose comments helped to improve the manuscript. The paper was supported by NASA Earth and Space Science Fellowship NNX08AX04H and partially supported by NASA grant NNX08AH32G.

---

\* Electronic address: rshcherbakov@cfa.harvard.edu;  
URL: <http://www.cfa.harvard.edu/~rshcherb/>

- <sup>1</sup> A. Panaitescu and P. Kumar, *Astrophys. J.* **571**, 779 (2002).  
<sup>2</sup> J. F. C. Wardle, D. C. Homan, R. Ojha, and D. H. Roberts, *Nature* **395**, 457 (1998).  
<sup>3</sup> F. Yuan, E. Quataert, and R. Narayan, *Astrophys. J.* **598**, 301 (2003).  
<sup>4</sup> F. Xiao, C. Shen, Y. Wang, H. Zheng and S. Wang, *J. Geophys. Res.* **113**, 05203 (2008).  
<sup>5</sup> M. Maksimovic, V. Pierrard and J. F. Lemaire, *A&A* **324**, 725 (1997).  
<sup>6</sup> J. Bergman and B. Eliasson, *Phys. Plasmas* **8**, 1482 (2001).  
<sup>7</sup> R. Schlickeiser, *Physica Scripta* **75**, 33 (1998).  
<sup>8</sup> R. Schlickeiser, *Phys. Plasmas* **2**, 4025 (1995).  
<sup>9</sup> K. Imre, *Phys. Fluids* **5**, 459 (1962).  
<sup>10</sup> D. B. Melrose, *Quantum plasmadynamics: unmagnetized plasmas* (Springer, New York, 2008).

- <sup>11</sup> L. D. Landau and E. M. Lifshits, *Physical Kinetics* (Pergamon Press, Oxford, 1980).  
<sup>12</sup> J. D. Jackson, *J. Nucl. Energy, Part C* **1**, 171 (1960).  
<sup>13</sup> D. B. Melrose, R. C. McPhedran, *Electromagnetic Processes in Dispersive Media*, (Cambridge University Press: Cambridge, 1991), p.283.  
<sup>14</sup> F. Xiao, *Pl. Phys. and Cont. Fus.* **48**, 203 (2006).  
<sup>15</sup> R. L. Mace and M. A. Hellberg, *Phys. Plasmas* **2**, 2098 (1995).  
<sup>16</sup> B. A. Trubnikov, Thesis, Moscow Institute of Engineering and Physics (1958) [English translation in AEC-tr-4073, US Atomic Energy Commission, Oak Ridge, Tennessee, 1960].  
<sup>17</sup> W. J. Liu, P. F. Chen, M. D. Ding, and C. Fang, "Energy spectrum of the electrons accelerated by reconnection electric field: exponential or power-law?", submitted to *Astrophys. J.* .